

## Synthesis and Characterization of A Fascinating Coordination Polymer Metal-Organic Framework Featuring Cobalt (II) and 4,4'-Bipyridine

Cepi Kurniawan\*

Chemistry Department, Faculty of Mathematics and Natural Sciences, Universitas Negeri Semarang, Semarang 50229, Indonesia

\*Corresponding author email: [kurniawan.cepi@mail.unnes.ac.id](mailto:kurniawan.cepi@mail.unnes.ac.id)

Received July 11, 2023; Accepted March 05, 2024; Available online July 20, 2024

**ABSTRACT.** This investigation delineates the fabrication, comprehensive characterization, and electrochemical evaluation of a one-dimensional Cobalt-based Metal-Organic Framework (Co-MOFs), constructed from 4,4'-Bipyridine ligands and Cobalt (II) ions. The study aimed to perfect the synthesis protocol, elucidate the structural and compositional attributes of the resultant MOF, and probe its electrochemical performance. Utilizing the reflux method, renowned for its efficacy and eco-compatibility, we synthesized the MOF and affirmed its formation through a suite of analytical techniques, including Infrared (IR) spectroscopy, Ultraviolet-Visible (UV-Vis) spectroscopy, Atomic Absorption Spectroscopy (AAS), and electrical conductivity measurements. The synthesized Co-MOFs, chemically notated as  $[\text{Co}_2(4,4'\text{-bpy})_2(\text{SO}_4)(\text{H}_2\text{O})_2]\text{SO}_4 \cdot \text{H}_2\text{O}$ , manifested as a one-dimensional coordination polymer. X-ray Diffraction (XRD) analysis unveiled its monoclinic crystallinity within the  $C_2$  space group. Electrochemical characterization uncovered a reversible redox system, evidenced by a robust peak current ratio ( $I_{\text{pa}}/I_{\text{pc}} = 7.5$ ), indicative of efficient electron transfer processes. Furthermore, the Co-MOFs significantly augmented the kinetics of the oxygen evolution reaction (OER) in an alkaline aqueous solution, highlighting its potential as a superior catalyst in energy-related electrochemical applications. This work not only contributes to the field of MOF synthesis but also sets the stage for future explorations into their practical applications in sustainable energy systems.

**Keywords:** Electrochemical properties, metal-organic framework, oxygen evolution reaction catalyst, 4,4'-bipyridine.

### INTRODUCTION

Metal-organic framework (MOF), recognized as porous coordination polymers, represent a class of crystalline materials formed through the coordination of metal ions and organic ligands. Their structural versatility, dictated by the arrangement of organic ligands, allows for one, two, or three-dimensional frameworks, paving the way for a myriad of applications (Horike et al., 2020; Kempahanumakkagari et al., 2018; Tranchemontagne et al., 2009). MOFs are distinguished by their extraordinary porosity, often reaching up to 90%, and their substantial internal surface area, sometimes exceeding  $10,000 \text{ m}^2/\text{g}$ —a stark contrast to traditional adsorbents like activated carbon (Anisuzzaman et al., 2015). Their low density and high crystallinity further amplify their appeal for various applications (Ranocchiari & van Bokhoven, 2011).

Synthesis of MOFs is typically executed through liquid-phase methods, where metal ions and ligands are combined in solution or where a solvent is introduced to a mix of metal solids and ligands. Established methods include hydrothermal, solvothermal, microwave-assisted, and sonochemical

approaches, each with its unique advantages and limitations (Dey et al., 2014; Hu et al., 2020; Hosseini & Tadjarodi, 2022; Mendes et al., 2020; Wei et al., 2021). However, this research adopts the reflux method, a less conventional but efficient technique in MOF synthesis. Characterized by the condensation of vapor and the return of the condensate to the system, the reflux method offers several benefits, including lower cost, environmental compatibility, reduced synthesis time compared to hydrothermal or solvothermal methods, and adaptability for large-scale production (Liang et al., 2018).

In 2020, Saelim and co-workers investigated the formation of Cobalt-based MOF with bipyridine and hydroxybenzoate ligands. They reported that the bipyridine ligand can act as a bridging ligand to connect Cobalt dinuclear units and the mononuclear Co(II) chromophores, providing a one-dimensional alternating zigzag chain-like structure (Saelim et al., 2020). A similar result was also reported by Mauger-Sonnk and coworkers (2014) with advanced findings on the adsorption of water due to the labile binding of water ligands and cobalt (Mauger-Sonnk et al., 2014). The Cobalt-based MOFs, in particular, have garnered significant interest due to their unique

electrochemical properties. Cobalt's variable oxidation states and the ability to participate in electron transfer reactions make these MOFs highly effective in electrochemical applications. These include energy storage, catalysis, and sensing (Dey et al., 2023). For instance, research by Liu et al. (2023) demonstrated how Cobalt-based MOFs could be utilized in supercapacitors, highlighting their remarkable capacitance and stability (Liu et al., 2016). Similarly, a study explored the role of Co-MOFs in electrocatalysis, revealing their potential in water splitting and oxygen reduction reactions (Tripathy et al., 2019).

This study aims to delve into the synthesis, structural analysis, and exploration of the electrochemical properties of a novel one-dimensional coordination polymer compound based on Cobalt(II) and 4,4'-bipyridine. The specific focus on Cobalt(II) in MOFs is driven by the metal's unique characteristics, which include versatile coordination environments and redox properties. These features make Co-based MOFs particularly intriguing for applications in areas such as gas storage, catalysis, and electrochemical sensing. Despite the growing interest in MOFs, Co-based MOFs, especially those incorporating 4,4'-bipyridine, remain relatively unexplored. This study seeks to bridge this gap by synthesizing and characterizing this unique MOF, thereby contributing to the expanding field of MOF research. Our approach underscores the potential of Co(II)-4,4'-bipyridine MOFs in electrochemical applications, aligning with the increasing demand for efficient and sustainable materials in energy storage and conversion technologies.

## EXPERIMENTAL SECTION

### Material

The materials utilized include cobalt (II) sulfate heptahydrate from R&M Chemicals, 4,4'-bipyridine from Wako, Whatman filter paper (#42), dimethyl sulfoxide (DMSO), dimethylformamide (DMF), n-hexane, acetonitrile, distilled water, and alcohol, all procured from Merck. These chemicals are of analytical grade and were used as received, without any additional purification.

### Synthesis Compound

One-dimensional polymeric compound  $[\text{Co}_2(4,4'\text{-bpy})_2(\text{SO}_4)(\text{H}_2\text{O})_2]\text{SO}_4 \cdot \text{H}_2\text{O}$  (1) was synthesized using the following procedure (Hosoya et al., 2016; Prior et al., 2011). A mixture of 4,4'-bipyridine (bpy; 1.56 g; 10 mmol),  $\text{CoSO}_4 \cdot 7\text{H}_2\text{O}$  (2.81 g; 10 mmol), and acetone (50 mL) was prepared. The pH of the mixture was adjusted to 6. The mixture solution was then placed in a boiling three-neck flask equipped with a magnetic stirrer and a condenser. The solution was refluxed at 60 °C for 2 hours, resulting in the formation of a pink solution. Subsequently, distilled water (50 mL) was added to the solution with continuous stirring, leading to the

immediate formation of a purple-pink precipitate. The precipitate was allowed to stir slowly for 30 minutes, filtered, and washed with acetone and cold distilled water. Finally, the precipitate was dried.

### Compound Characteristics

For IR analysis, the MOF was finely ground and mixed with potassium bromide (KBr) in a 1:100 ratio to form a homogenous mixture. This mixture was then pressed into transparent, thin pellets under high pressure. These pellets were analyzed using a Perkin Elmer Spectrum-100 IR spectrometer in the range of 4000-400  $\text{cm}^{-1}$ , providing insights into the functional groups present in the MOF. Next, 10  $\mu\text{g}$  of the Co-MOFs was dissolved in a 5 mL dimethyl formamide (DMF) solvent. The solution was then subjected to spectral analysis using a Spectroquant Pharo 300 UV-Vis spectrophotometer, covering a wavelength range of 200-900 nm.

The MOF sample, reduced to a fine powder, was evenly spread over a flat, non-reflective sample holder. This preparation was crucial to avoid preferential orientation and to obtain a representative diffraction pattern. The sample was then analyzed using a PANalytical X'Pert<sup>3</sup> Powder diffractometer, with measurements taken at angles ranging from 10° to 80°. The diffractogram was then refined using Rietica to extract the parameter cells.

The MOF was subjected to acid digestion using a mixture of nitric acid and hydrogen peroxide, followed by dilution with deionized water, to prepare a solution suitable for metal content analysis. This solution was then analyzed using a Shimadzu AA-6800 Automatic Absorption Spectrophotometer. For measuring ionic conductivity, the MOF was compacted into a pellet and placed between two electrodes in a Mettler TGA Conductometer SDTA 851°. The uniform thickness and diameter of the pellet were ensured for accurate conductivity readings. Further, 10  $\mu\text{g}$  of the Co-MOFs was weighed and placed in the sample holder of a Sherwood Magnetic Susceptibility Balance (MSB), employing the Gouy Method. This approach was instrumental in understanding the magnetic properties of the Co(II) centers in the MOF.

The Co-MOFs were dispersed in ethanol (5 mg/10 mL) and ultrasound for 3 hours. For electrochemical measurements, the dispersed Co-MOFs were immobilized on a glassy carbon electrode (GCE) surface 5  $\mu\text{L}$  and dried for 24 hours at room temperature. The three-electrode system was used with Ag/AgCl and Pt as reference electrodes and counter electrodes respectively. The aqueous solution of  $\text{KClO}_4$  was used as an electrolyte to study the electroactivity of Co-MOFs and the aqueous solution of KOH was used as an electrolyte in oxygen evolution electrocatalytic activities. Voltammograms were obtained through this setup using a Rodheostat Potentiostat, providing a detailed analysis of the redox properties of the MOF.

## RESULT AND DISCUSSION

### Synthesis of Complex Compound

Synthesis of Co-MOFs is performed using the reflux method. Reflux is a synthesis method based on the solution. This method includes a synthesis that applies green synthesis. The advantage of this is a simple method, the use of relatively low (Aditha et al., 2016), and produce products that are not dangerous (Fatimah & Faridhatunnisa, 2017). This reflux synthesis produced a light purple-pink precipitate weighing 3.5632 g (yield of 52.68%) and a crystal of 0.22 g, as shown in **Figure 1**.

The observations of MOF Co-Bpy products are presented in **Figure 2**, showcasing the morphology analysis of Co-MOFs powder using SEM. Figure 2 (a) shows a broad view of the MOF structure, which

appears to have an agglomerated morphology with clumps of rod-like and blocky crystals densely packed together. The surface is rough and heterogeneous, with a variety of shapes and sizes in the crystal formation. There are no distinct or well-formed crystals, suggesting a somewhat disordered crystallization process or a polycrystalline nature. At a higher magnification, we can observe finer details of the material. Here, individual rod-like crystals and their junctions are more clearly visible. They are tightly intergrown, with dimensions annotated on the image. The lengths of these features range from approximately 1.3 to 2.7 micrometers, and they display a more uniform and orderly arrangement. This close-up view allows us to appreciate the surface texture and the interlocking nature of the crystals.



**Figure 1.** Powder and crystal of Co-MOF compound

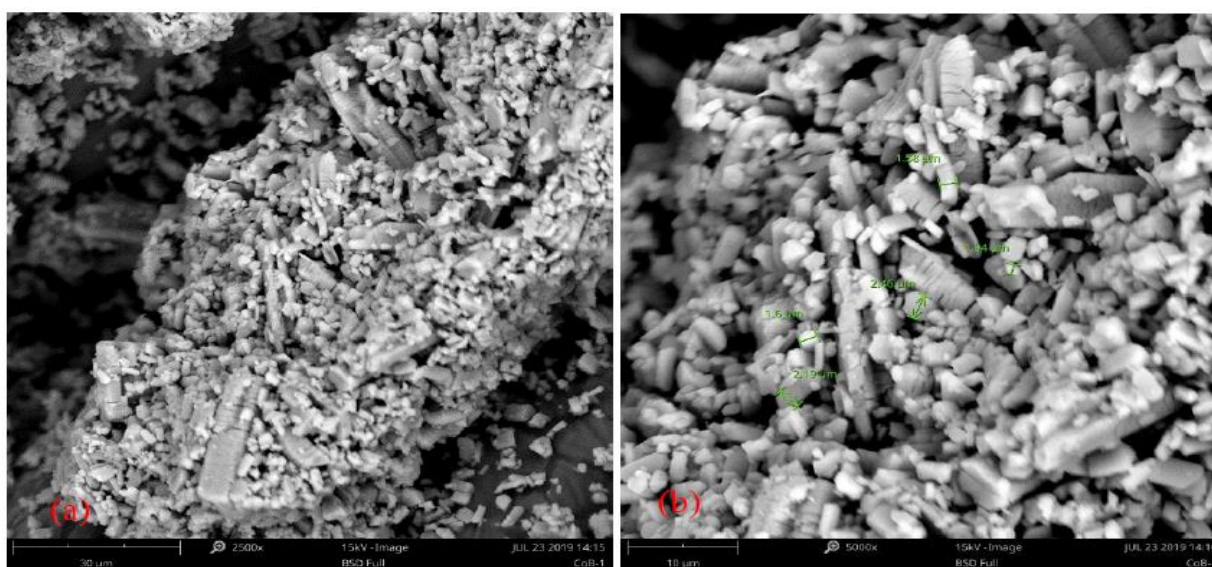


**Figure 2.** Morphology of Co<sup>II</sup>(Bipy) under scanning electron microscope.

The magnetic susceptibility analysis results of Coll compounds (4,4'-bpy) revealed an effective magnetic moment ( $\mu_{\text{eff}}$ ) of 5.43 BM. Typically, cobalt (II) coordination with octahedral structures in high spin states exhibits an effective magnetic moment value ( $\mu_{\text{eff}}$ ) ranging from 4.3 to 5.2 BM (Figgis & Nyholm, 1954; Szafran et al., 1991). Thus, it can be inferred that the Co-MOFs compound possesses an octahedral structure and is paramagnetic due to its high spin state. In contrast, the coordination of Cobalt (II) with three unpaired electrons in octahedral coordination is theoretically expected to have a magnetic moment ( $\mu_s$ ) of 3.87 BM. This indicates an excess of the effective magnetic moment compared to the theoretical magnetic moment. This excess can be attributed to orbital contributions in the octahedral geometry. In octahedral fields, the d orbitals split into  $e_g$  and  $t_{2g}$ . The electron configuration of the  $\text{Co}^{2+}$  metal ion is  $d^7$ . Based on the magnetic moment data,  $\text{Co}^{2+}$  metal ions exhibit a high spin state, resulting in the electron configuration of  $t_{2g}^5 e_g^2$ . In the  $t_{2g}^5$  configuration, the possible configurations include  $(d_{xy})^2(d_{xz})^2(d_{yz})^1$  or  $(d_{xy})^1(d_{xz})^2(d_{yz})^2$  or  $(d_{xy})^2(d_{xz})^1(d_{yz})^2$ . It is this configuration change that contributes to the orbital contribution in the effective magnetic moment of the coordination compound (Sugiyarto, 2012).

Characterization through UV-Vis was performed by preparing a sample solution with a concentration of  $10^{-3}$  M in DMSO because the ligand is not dissolved in water. The objective of this characterization was to identify newly formed compounds based on the appearance of absorbance peaks at specific wavelengths. **Figure 2** illustrates the UV-Vis spectra of Co-MOFs and 4,4'-bpy in DMSO.

From the spectra depicted in **Figure 3**, it is evident that a new absorbance peak emerges in the compound Co-MOFs, indicating the formation of new compounds during synthesis. At a wavelength of 271 nm, an interligand transition  $\pi \rightarrow \pi^*$  originating from the 4,4'-bpy ligands is observed (Dikhtiarenko et al., 2016). Additionally, an absorbance band at 343 nm signifies the MLCT (Metal Ligand Charge Transfer) transition of  $\text{Co}(d\pi) \rightarrow 4,4'\text{-bpy}(\pi^*)$  (Kumar et al., 2015). Furthermore, the absorbance band at 544 nm indicates a  $d-d$  transition in  $\text{Co}^{2+}$  metal due to the presence of unfilled d orbitals (Arab Ahmadi et al., 2013).

FTIR characterization was conducted using KBr pellets, and the measurements were taken within the wavenumber range of 400-4000  $\text{cm}^{-1}$ . The purpose of this analysis was to identify the formation of new compounds by examining specific functional groups. **Figure 4** displays the FTIR spectra of Co-MOFs and 4,4'-bpy, with the IR spectrum of 4,4'-bpy serving as a comparison.

From all the spectra presented in **Figure 4**, it can be observed that the intense strong peak around 3028  $\text{cm}^{-1}$  corresponds to C-H vibrations observed in 4,4'-bpy. This peak did not appear when the Co-MOFs

formed. However, the broad peak at around 3446  $\text{cm}^{-1}$  is interpreted as OH vibration from water molecules in Co-MOFs. Specific vibrations of 4,4'-bpy, such as C=N, C=C, and C-H aromatic rings, are observed at 1596, 1410, and 1219  $\text{cm}^{-1}$ , respectively. In Co-MOFs, these vibrations are detected at 1607, 1415, and 1224  $\text{cm}^{-1}$  for the crystalline form. For the powder form of Co-MOFs, the vibrations occur at 1607, 1414, and 1223  $\text{cm}^{-1}$  (Topaçlı & Akyüz, 1995). Notably, these data indicate that the vibrations of C=N, C=C, and C-H aromatic rings experience a shift towards higher wavenumbers, indicating the formation of Co-MOFs due to the coordination between Cobalt (II) metal and 4,4'-bpy ligands (Czakis-Sulikowska et al., 2001). The S-O vibration from sulfate moiety was observed as the strong peaks at wavenumbers 1111  $\text{cm}^{-1}$ . This confirms the presence of sulfates acting as ligands in the formation of Co-MOFs. Another noteworthy peak occurs in the IR spectra of Co-MOFs, this peak indicates the presence of a metal bond with 4,4'-bpy (Co-N bond) that appears at 620  $\text{cm}^{-1}$ . It is worth mentioning that 4,4'-bpy exhibits a sensitive band at 613  $\text{cm}^{-1}$ , which tends to shift towards higher wavenumbers upon coordination with a metal (Baran & Lii, 2003). Another peak at 804  $\text{cm}^{-1}$  is also related to Co-N interaction as it is in agreement with Kim and coworkers (2022) who study the coordination of Cobalt with  $\text{NH}_3$  (Kim et al., 2022).

The metal content analysis was performed using AAS and the analysis revealed a cobalt metal content of 17.46%. Subsequent analysis led to the proposed formula  $[\text{Co}_2(\text{C}_{10}\text{N}_2\text{H}_8)_2(\text{SO}_4)]\text{SO}_4 \cdot 2\text{H}_2\text{O}$ , with a cobalt metal content of 17.8% (theoretical metal content). In advance, the conductometer analysis was conducted to determine the ions dissolved in the sample solution based on their conductivity values. Higher conductivity values indicate a higher concentration of dissolved ions in the solution. The respective conductivity values for the solutions are provided in **Table 1**.

Based on the information provided in Table 1, it is evident that the compound  $[\text{Co}_2(4,4'\text{-bpy})_2(\text{SO}_4)]\text{SO}_4 \cdot 2\text{H}_2\text{O}$  exhibits a conductivity value of 22  $\text{Scm}^2\text{mol}^{-1}$ . Interestingly, this conductivity value aligns closely with that of  $\text{CuSO}_4$ , which is 22.4  $\text{Scm}^2\text{mol}^{-1}$ . There are the inner sphere and outer sphere  $\text{SO}_4^{2-}$  ions that contribute to the conductivity of Co-MOFs. Therefore, it is plausible to suggest that Co-MOFs or  $[\text{Co}_2(4,4'\text{-bpy})_2(\text{SO}_4)]\text{SO}_4 \cdot \text{H}_2\text{O}$  has the potential to dissolve in water, forming two ions:  $[\text{Co}_2(4,4'\text{-bpy})_2(\text{SO}_4)]^{2+}$  and  $(\text{SO}_4)^{2-}$ .

Subsequently, XRD analysis was conducted to determine the crystal structure of the samples. The crystal structure was further analyzed using the Rietveld method through Rietica software (Hunter, 2000). This analysis was based on the crystal data of the previously reported 1D coordination polymer  $[(\text{Cd}(\mu\text{-}4,4'\text{-}4,4'\text{-bpy})(4,4'\text{-bpy})_2(\text{H}_2\text{O})_2)(\text{NO}_3)_2] \cdot 2 \cdot 4,4'\text{-bpy} \cdot 4.5 \text{H}_2\text{O}]_n$  (Seidel et al., 2011). The results of the refinement can be observed in **Figure 4**.

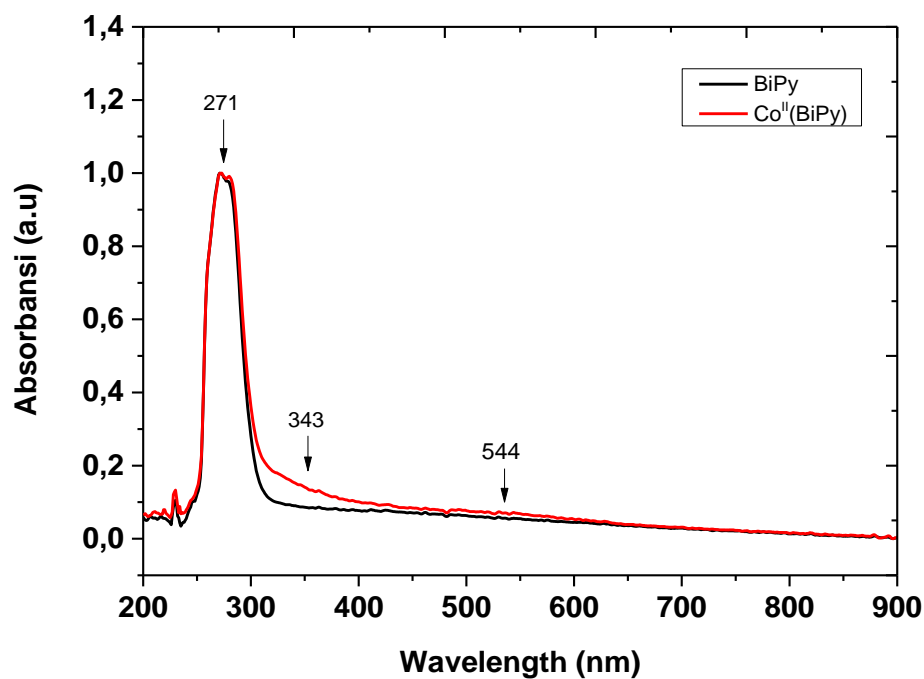


Figure 3. UV-Vis Spectra of Co-MOFs and 4,4'-bpy.

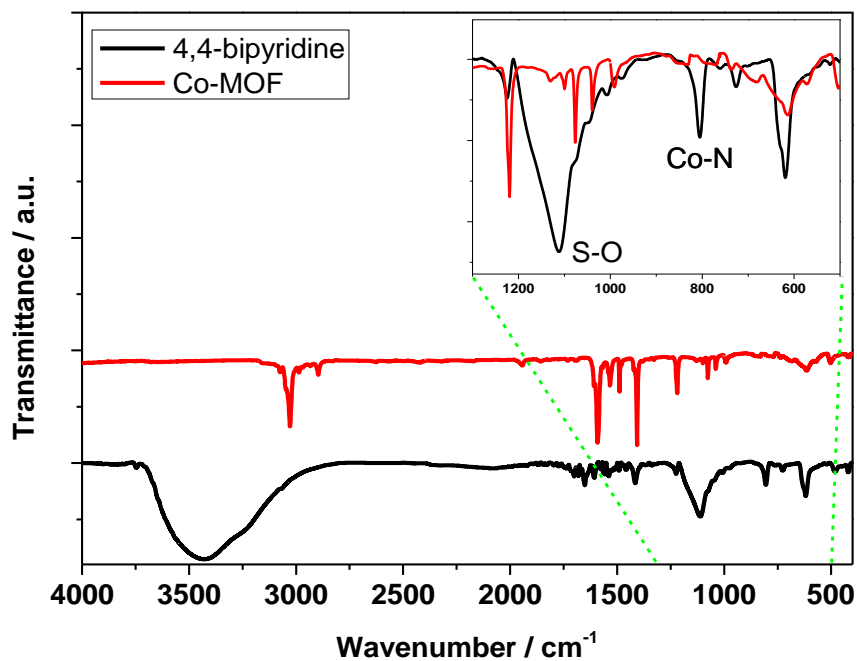
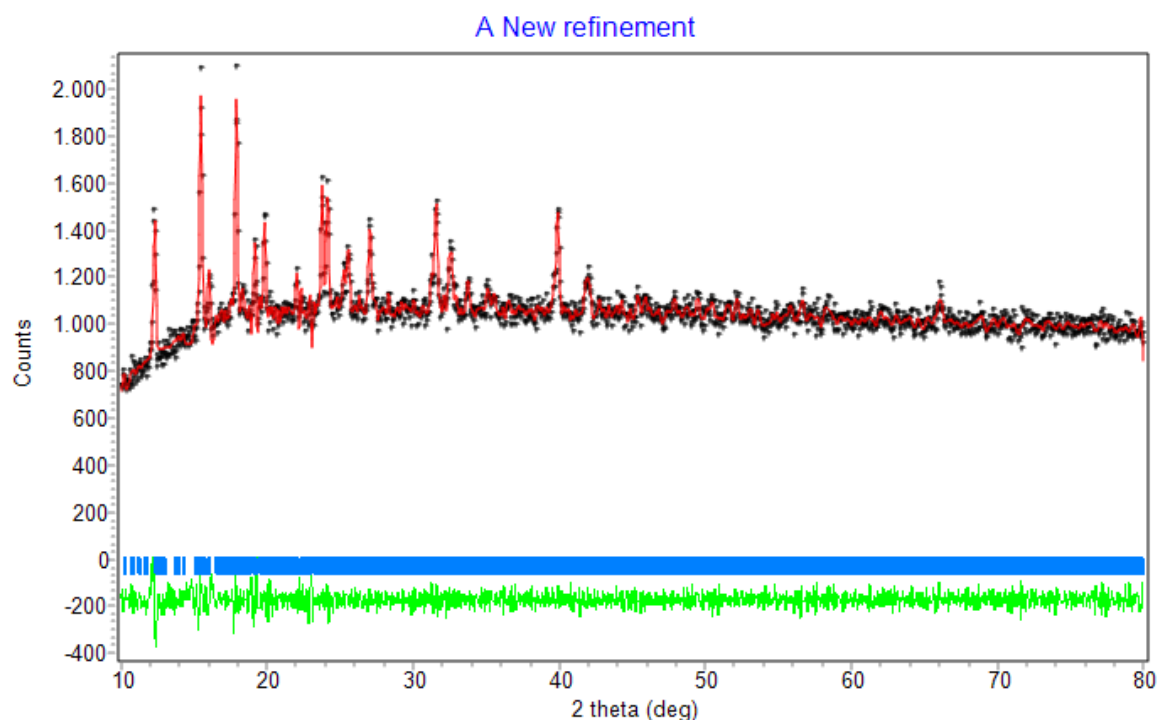


Figure 4. IR Spectra of Co-MOFs (red line) and 4,4'-bpy (black line). The onset shows a magnified wavelength.

Table 1. Conductivity of complex compound in water

compound	Conductivity Scm <sup>2</sup> mol <sup>-1</sup>	( $\Lambda m$ )	Cation:Anion ratio	Number of ions
NaCl	23,6		1:1	2
CuSO <sub>4</sub>	22,4		1:1	2
CuCl <sub>2</sub>	28,9		2:1	3
AlCl <sub>3</sub>	74,9		3:1	4
Co-MOFs	22		1:1	2



**Figure 5.** illustrates the plot results obtained from the Rietveld analysis using Rietica for the compound Co-MOFs.

The black dot sign represents X-ray diffraction observations, while the red line represents calculated data. The blue vertical line indicates the expected Bragg position and the horizontal green line represents the disparity between the calculated results and X-ray diffraction observations. **Figure 5** demonstrates a resemblance between the crystallographic properties of Co-MOFs in comparison with the parameter cell of the compound  $[(\text{Cd}(\mu\text{-}4,4'\text{-}4,4'\text{-bpy})(4,4'\text{-bpy})_2(\text{H}_2\text{O})_2)(\text{NO}_3)_2 \cdot 24,4'\text{-bpy} \cdot 4.5 \text{H}_2\text{O}]_n$ . The structure exhibits a monoclinic crystal system and belongs to the C 2 space group, characterized by crystal parameters:  $a = 17.904 \text{ \AA}$ ,  $b = 11.753 \text{ \AA}$ ,  $c = 49.68 \text{ \AA}$ ,  $\beta = 94.68^\circ$ ,  $V = 10,453.28 \text{ \AA}^3$ . The goodness-of-fit (GoF) value is 2,138, while the  $R_p$  and  $R_{wp}$  values are 2,427 and 4,290, respectively. These parameters are deemed acceptable as the GoF value is less than 4% and  $R_{wp}$  value is less than 20%. A plausible structure for Co-MOFs is depicted in **Figure 6**. The voltammogram of Co-MOFs modified GCE is shown in **Figure 5**. It is observed that the black curve for the GCE shows no such peaks, indicating that the bare electrode does not facilitate the redox process under the same conditions. This can be due to a lack of electroactive sites or a potential range that does not favor the redox activity of any species adsorbed or present at the GCE surface. However, the Co-MOFs/GCE shows a pair of redox peaks, indicative of a reversible electrochemical reaction. The reduction peak appears at an anodic peak potential ( $E_{pa}$ ) of 120 mV with a peak current density ( $I_{pa}$ ) of  $30 \mu\text{A}/\text{cm}^2$ . This peak is associated with the reduction of Co(II) to Co(I), indicating that the Co-MOFs is acting

as an electroactive material facilitating this redox reaction. The corresponding oxidation peak occurs at a cathodic peak potential ( $E_{pc}$ ) of -25 mV with a peak current density ( $I_{pc}$ ) of  $-8 \mu\text{A}/\text{cm}^2$ . This peak represents the reverse process, where Co(I) is being oxidized back to Co(II). The presence of these peaks in the Co-MOFs/GCE but not in the GCE suggests that the Co-MOFs provide active sites for the redox reaction, which are not present on the bare glassy carbon electrode. The reversibility demonstrates the stability of the analyte during the reduction reaction, allowing for subsequent oxidation (Elgrishi et al., 2017).

The separation between the anodic and cathodic peak potentials ( $\Delta E_p$ ) is related to the kinetics of the electron transfer process. A smaller  $\Delta E_p$  indicates a faster electron transfer and a more reversible reaction. In this case, the  $\Delta E_p$  can be calculated as  $120 \text{ mV} - (-25 \text{ mV}) = 145 \text{ mV}$ , which, if close to the theoretical  $59/n \text{ mV}$  (where  $n$  is the number of electrons transferred in the rate-determining step) at room temperature, would suggest a relatively fast and reversible electron transfer process for the Co(II)/Co(I) couple in the Co-MOFs/GCE system. The magnitude of  $\Delta E$  depends on the barrier or obstacle. If there is a higher barrier to electron transfer, the electron transfer reaction proceeds slowly, and a larger negative (or positive) potential is required for the reduction (or oxidation) reaction, resulting in a larger value of  $\Delta E$  (Elgrishi et al., 2017). Based on the electrochemical parameters, the ratio of the anodic peak to the cathodic peak is approximately 7.5 ( $I_{pa} / I_{pc} \approx 7.5$ ). This indicates that the cyclic voltammogram exhibits a quasi-reversible system (Oh & Chang, 2016).

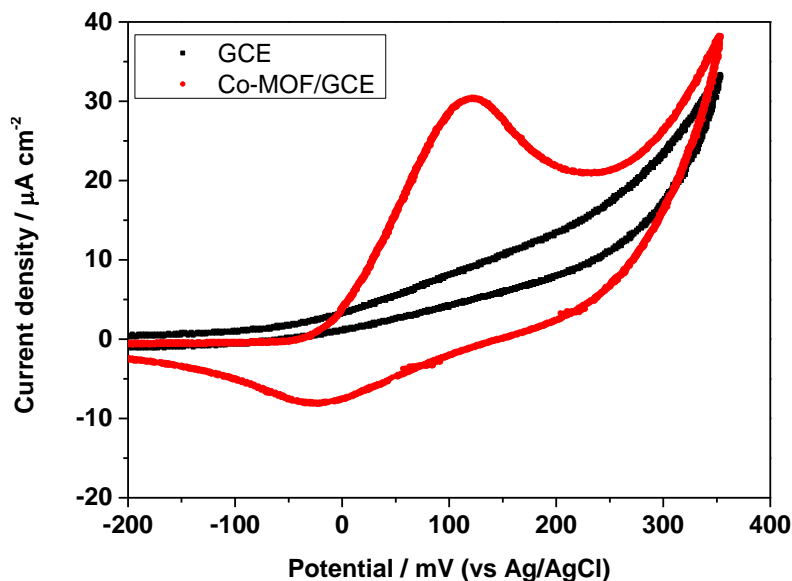


**Figure 6.** The voltammogram of the Co-MOFs 0,5 M KClO<sub>4</sub> aqueous solution recorded at a scan rate of 100 mVs<sup>-1</sup>.

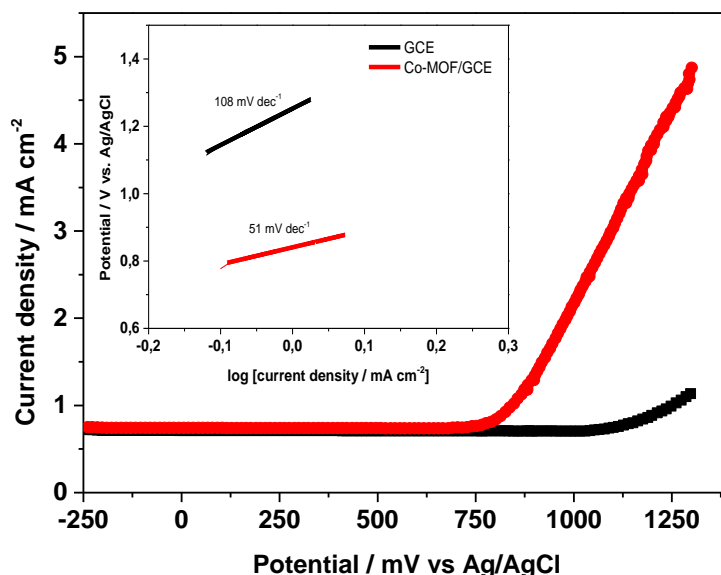


**Figure 7.** Tafel plots comparing the electrocatalytic performance for the oxygen evolution reaction of GCE (black line) and Co-MOFs/GCE (red line) in a 0.5 M KOH aqueous solution at a scan rate of 5 mVs<sup>-1</sup>.

The oxygen evolution electrocatalytic activity of Co-MOFs was investigated using linear sweep voltammetry (LSV) under 0,5 M KOH aqueous solution and a scan rate of 5 mVs<sup>-1</sup>. The LSV is shown in **Figure 7**. From the linear sweep voltammogram, we can observe the electrocatalytic activity of both the GCE and the Co-MOFs/GCE. As stated, the current density for the Co-MOFs/GCE is 4.5 mA/cm<sup>2</sup> at a potential of 1250 mV versus Ag/AgCl, which is significantly higher than the GCE (1 mA/cm<sup>2</sup>) at the same potential. This indicates that the Co-MOF modification greatly enhances the electrocatalytic performance of the GCE for OER, likely due to the increased active surface area and the presence of catalytically active sites within the MOF structure.

Regarding the Tafel plot, the Tafel slope is an indicator of the kinetics of the electrochemical reaction. The Tafel slope for the GCE is 108 mV/dec, which is more than double the Co-MOFs/GCE's slope of 51 mV/dec. A lower Tafel slope indicates a faster reaction rate and suggests that the reaction mechanism may be different or more efficient. Specifically, the Tafel slope can give insights into the number of electrons involved in the rate-determining step of the reaction and the reaction's dependence on overpotential. A Tafel slope of 51 mV/dec for the Co-MOFs/GCE suggests that the electrocatalytic process for OER on this modified electrode is highly efficient, with a reaction mechanism that allows for faster kinetics compared to the unmodified GCE. It implies

that the Co-MOF modification reduces the energy barrier for the reaction, possibly by providing more favorable intermediate steps or by altering the reaction pathway to one that is more efficient. Also, the Tafel plot onset further suggests that the Co-MOFs/GCE requires less overpotential to reach a given current density compared to the bare GCE, which is consistent with the enhanced performance observed in the voltammogram.

## CONCLUSIONS

The synthesis of a cobalt-based Metal-Organic Framework (Co-MOFs) utilizing the reflux method with cobalt (II) and 4,4'-bipyridine (bpy) ligand has been successfully conducted. This process achieved a commendable yield of 52.68%, and facilitated the growth of a substantial big crystal weighing 0.22 grams. X-ray crystallography confirmed that the resulting compound crystallizes in the monoclinic system and is classified within the  $C_2$  space group. Notably, the electrochemical analysis revealed that these Co-MOFs possess a robust reversible redox system, characterized by well-defined cyclic voltammetry peaks with a peak-to-peak separation ( $\Delta E_p$ ) of approximately 145 mV. This electrochemical feature suggests efficient electron transfer capabilities, which is further corroborated by the enhanced activity observed for the oxygen evolution reaction (OER) in an alkaline medium. The synthesized Co-MOFs demonstrate promising potential for catalytic applications, particularly in energy conversion and storage systems.

## ACKNOWLEDGEMENTS

The author would like to thank Universitas Negeri Semarang for providing research funding.

## REFERENCES

- Aditha, S. K., Kurdekar, A. D., Chunduri, L. A., Patnaik, S., & Kamiseti, V. (2016). Aqueous based reflux method for green synthesis of nanostructures: application in czts synthesis. *MethodsX*, *3*, 35–42. <https://doi.org/10.1016/j.mex.2015.12.003>
- Anisuzzaman, S. M., Joseph, C. G., Taufiq-Yap, Y. H., Krishnaiah, D., & Tay, V. V. (2015). Modification of commercial activated carbon for the removal of 2,4-dichlorophenol from simulated wastewater. *Journal of King Saud University - Science*, *27*(4), 318–330. <https://doi.org/10.1016/j.jksus.2015.01.002>
- Ahmadi, R.A., Hasanvand, F., Bruno, G., Amiri Rudbari, H., & Amani, S. (2013). Synthesis, spectroscopy, and magnetic characterization of copper(II) and cobalt(II) complexes with 2-amino-5-bromopyridine as ligand. *ISRN Inorganic Chemistry*, *2013*, 1–7. <https://doi.org/10.1155/2013/426712>
- Baran, E. J., & Lii, K.-H. (2003). Vibrational spectra of the layered compound  $[(VO_2)_2(4,4\text{-bipy})_{0.5}(4,4'\text{-Hbipy})(PO_4)] \cdot H_2O$ . *Zeitschrift für Naturforschung B*, *58*(5), 485–488. <https://doi.org/10.1515/znb-2003-0520>
- Czakis-Sulikowska, D., Czylkowska, A., & Malinowska, A. (2001). Some dn metal complexes with 4,4'-bipyridine and trichloroacetates. preparation, characterization and thermal properties. *Journal of Thermal Analysis and Calorimetry*, *65*(2), 505–513. <https://doi.org/10.1023/a:1012493406026>
- Dey, B., Ahmad, M. W., Kim, B. H., Kamal, T., Yang, D. J., Patra, C. N., Hossain, S. K. S., Choudhury, A. (2023). Manganese cobalt-MOF@carbon nanofiber-based non-enzymatic histamine sensor for the determination of food freshness. *Analytical and Bioanalytical Chemistry*, *415*(17), 3487–3501. <https://doi.org/10.1007/s00216-023-04737-0>
- Dey, C., Kundu, T., Biswal, B. P., Mallick, A., & Banerjee, R. (2014). Crystalline metal organic frameworks (MOFs): Synthesis, structure and function. *Acta Crystallographica Section B: Structural Science, Crystal Engineering and Materials*, *70*, 3–10. <https://doi.org/10.1107/S2052520613029557>
- Dikhtiarenko, A., Villanueva-Delgado, P., Valiente, R., Garcia, J. R., & Gimeno, J. (2016). Tris(bipyridine)metal(II)-templated assemblies of 3D alkali-ruthenium oxalate coordination frameworks: crystal structures, characterization and photocatalytic activity in water reduction. *Polymers*, *8*(2), 48. <https://doi.org/10.3390/polym8020048>
- Elgrishi, N., Rountree, K. J., McCarthy, B. D., Rountree, E. S., Eisenhart, T. T., & Dempsey, J. L. (2017). A Practical beginner's guide to cyclic voltammetry. *Journal of Chemical Education*, *95*(2), 197–206. <https://doi.org/10.1021/acs.jchemed.7b00361>
- Fatimah, I., & Faridhatunnisa, A. (2017). Green synthesis of silver nanoparticle from photograph wastewater using hylocereus undatus skin extract. *Oriental Journal of Chemistry*, *33*(3), 1235–1240. <https://doi.org/10.13005/ojc/330322>
- Figgis, B. N., & Nyholm, R. S. (1954). Magnetic moments and stereochemistry of cobaltous compounds. *Journal of the Chemical Society (Resumed)*, 1954, 12–15. <https://doi.org/10.1039/jr9540000012>
- Horike, S., Nagarkar, S. S., Ogawa, T., & Kitagawa, S. (2020). A new dimension for coordination polymers and metal-organic frameworks: towards functional glasses and liquids. *Angewandte Chemie International Edition*, *59*(17), 6652–6664. <https://doi.org/10.1002/anie.201911384>

- Hosoya, K., Nishikiori, S.-i., Takahashi, M., & Kitazawa, T. (2016). Spin-crossover behavior of hofmann-type-like complex  $\text{Fe}(4,4'-bipyridine) $\text{Ni}(\text{CN})_4 \cdot n\text{H}_2\text{O}$  depending on guest species. *Magnetochemistry*, 2 (1), 8. <https://doi.org/10.3390/magnetochemistry2010008>$
- Hu, Z., Kundu, T., Wang, Y., Sun, Y., Zeng, K., & Zhao, D. (2020). Modulated hydrothermal synthesis of highly stable MOF-808(Hf) for methane storage. *ACS Sustainable Chemistry & Engineering*, 8(46), 17042–17053. <https://doi.org/10.1021/acssuschemeng.0c04486>
- Hunter, B. (2000). Rietica-A visual Rietveld program.
- Karbalae Hosseini, A., & Tadjarodi, A. (2022). Sonochemical synthesis of nanoparticles of Cd metal organic framework based on thiazole ligand as a new precursor for fabrication of cadmium sulfate nanoparticles. *Materials Letters*, 322, 132481. <https://doi.org/10.1016/j.matlet.2022.132481>
- Kempahanumakkagari, S., Vellingiri, K., Deep, A., Kwon, E. E., Bolan, N., & Kim, K.-H. (2018). Metal-organic framework composites as electrocatalysts for electrochemical sensing applications. *Coordination Chemistry Reviews*, 357, 105–129. <https://doi.org/10.1016/j.ccr.2017.11.028>
- Kim, J., Kim, H. G., Kim, H. S., Dang Van, C., Lee, M. H., & Jeon, K. W. (2022). Facile gram-scale synthesis of  $\text{Co}_3\text{O}_4$  nanocrystal from spent lithium ion batteries and its electrocatalytic application toward oxygen evolution reaction. *Nanomaterials*, 13 (1), 125. <https://doi.org/10.3390/nano13010125>
- Kumar, P., Joshi, C., Srivastava, A. K., Gupta, P., Boukherroub, R., & Jain, S. L. (2015). Visible light assisted photocatalytic [3 + 2] azide-alkyne “click” reaction for the synthesis of 1,4-substituted 1,2,3-triazoles using a novel bimetallic Ru-Mn complex. *ACS Sustainable Chemistry & Engineering*, 4(1), 69–75. <https://doi.org/10.1021/acssuschemeng.5b00653>
- Liang, Y., Huang, H., Kou, L., Li, F., Lü, J., & Cao, H. L. (2018). Synthesis of metal-organic framework materials by reflux: A faster and greener pathway to achieve super-hydrophobicity and photocatalytic application. *Crystal Growth & Design*, 18(11), 6609–6616. <https://doi.org/10.1021/acs.cgd.8b00854>
- Liu, X., Shi, C., Zhai, C., Cheng, M., Liu, Q., & Wang, G. (2016). Cobalt-based layered metal-organic framework as an ultrahigh capacity supercapacitor electrode material. *ACS Applied Materials & Interfaces*, 8(7), 4585–4591. <https://doi.org/10.1021/acsami.5b10781>
- Mauger-Sonnek, K., Streicher, L. K., Lamp, O. P., Ellern, A., & Weeks, C. L. (2014). Structure control and sorption properties of porous coordination polymers prepared from  $\text{M}(\text{NO}_3)_2$  and 4,4'-bipyridine ( $\text{M}=\text{Co}^{2+}, \text{Ni}^{2+}$ ). *Inorganica Chimica Acta*, 418, 73–83. <https://doi.org/10.1016/j.ica.2014.04.025>
- Mendes, R. F., Rocha, J., & Almeida Paz, F. A. (2020). Chapter 8 - Microwave synthesis of metal-organic frameworks. In M. Mozafari (Ed.), *Metal-organic frameworks for biomedical applications* (pp. 159–176): Woodhead Publishing.
- Oh, S.-H., & Chang, B.-Y. (2016). A new accurate equation for estimating the baseline for the reversal peak of a cyclic voltammogram. *Journal of Electrochemical Science and Technology*, 7(4), 293–297. <https://doi.org/10.5229/JECST.2016.7.4.293>
- Prior, T. J., Yotnoi, B., & Rujiwatra, A. (2011). Microwave Synthesis and crystal structures of two cobalt-4,4'-bipyridine-sulfate frameworks constructed from 1-D coordination polymers linked by hydrogen bonding. *Polyhedron*, 30(2), 259–268. <https://doi.org/10.1016/j.poly.2010.10.010>
- Ranocchiaro, M., & van Bokhoven, J. A. (2011). Catalysis by metal-organic frameworks: fundamentals and opportunities. *Physical Chemistry Chemical Physics*, 13(14), 6388–6396. <https://doi.org/10.1039/c0cp02394a>
- Saelim, T., Chainok, K., Kielar, F., & Wannarit, N. (2020). Crystal structure of a novel one-dimensional zigzag chain-like cobalt(II) coordination polymer constructed from 4,4'-bipyridine and 2-hydroxy-benzoate ligands. *Acta Crystallographica Section E: Crystallographic Communications*, 76, 1302–1306. <https://doi.org/10.1107/S2056989020009482>
- Seidel, R. W., Goddard, R., Zibrowius, B., & Oppel, I. M. (2011). A molecular antenna coordination polymer from cadmium(II) and 4,4'-bipyridine featuring three distinct polymer strands in the crystal. *Polymers*, 3(3), 1458-1474. <https://doi.org/10.3390/polym3031458>
- Sugiyarto, K. H. (2012). *Dasar-dasar kimia anorganik transisi (Basics of transitional inorganic chemistry)*. Yogyakarta: Graha Ilmu.
- Szafran, Z., Pike, R., & Singh, M. (1991). *Microscale inorganic chemistry*. J. Wiley&Sons. Inc. New York.
- Topaçlı, A., & Akyüz, S. (1995). 4,4'-bipyridyl: vibrational assignments and force field. *Spectrochimica Acta Part A: Molecular and Biomolecular Spectroscopy*, 51(4), 633–641. [https://doi.org/10.1016/0584-8539\(94\)00159-9](https://doi.org/10.1016/0584-8539(94)00159-9)

- Tranchemontagne, D. J., Mendoza-Cortes, J. L., O'Keeffe, M., & Yaghi, O. M. (2009). Secondary building units, nets and bonding in the chemistry of metal-organic frameworks. *Chemical Society Reviews*, *38*(5), 1257–1283. <https://doi.org/10.1039/b817735j>
- Tripathy, R. K., Samantara, A. K., & Behera, J. N. (2019). A cobalt metal-organic framework (Co-MOF): a bi-functional electro active material for the oxygen evolution and reduction reaction. *Dalton Transactions*, *48*(28), 10557–10564. <https://doi.org/10.1039/c9dt01730e>
- Wei, R., Liu, Z., Wei, W., Liang, C., Han, G. C., & Zhan, L. (2021). Synthesis, crystal structure and characterization of two cobalt (ii) complexes based on pyridine carboxylic acid ligands. *Zeitschrift für anorganische und allgemeine Chemie*, *648*(9), e202000418. <https://doi.org/10.1002/zaac.202000418>